

Mitigation of Deceleration-Phase Rayleigh–Taylor Growth in Inertial Confinement Fusion Implosions

Y. Lawrence,^{1,2} V. N. Goncharov,² K. M. Woo,² W. Trickey,² and I. V. Igumenshchev²

¹University of Chicago

²Laboratory for Laser Energetics, University of Rochester

In inertial confinement fusion (ICF), small hot spots are desirable because they lower the threshold hot-spot energy required for ignition, $E_{\text{hs}} > 16 \text{ kJ } (R_{\text{hs}}/50 \text{ } \mu\text{m})^2$ (Refs. 1–4). However, they generally lead to greater implosion asymmetry due to the growth of the Rayleigh–Taylor (RT) instability on the inner shell surface during the deceleration phase. A challenge then arises of how to attain a high convergence ratio (CR, defined as the ratio of the initial inner shell radius to the hot-spot radius at peak compression), without excessively high RT growth. In this study we show that lowering the central density [by a factor of 5 or more compared to the vapor density of deuterium–tritium (DT) at triple point] has the greatest leverage in achieving small hot-spot sizes without excessive amplification of deceleration-phase RT.

First, we review some basic aspects of deceleration-phase RT growth. During the deceleration phase, initial perturbations on the inner shell surface grow exponentially because the less-dense hot spot pushes against the denser shell. Neglecting convergence effects and including only the instability drive term, $\Gamma_{\text{drive}} = \int \sqrt{A_T k g} dt$, where A_T is the Atwood number, g is the inner surface acceleration, and $k \cong \ell/R_{\text{hs}}$ is the effective wave number ℓ [the inner surface perturbations are decomposed in spherical harmonics with the mode number ℓ (see also Ref. 5)] and R_{hs} is the position of the shell's inner surface. We postpone defining A_T until later in this summary and assume for now that $A_T \cong 1$. Evaluating this integral from the start of the deceleration phase until peak compression (when the hot-spot radius reaches its minimum value $R_{\text{hs},m}$), it can be shown that $\Gamma_{\text{drive}} = \sqrt{2\ell} \operatorname{arcsinh}(\sqrt{\text{CR}_d - 1})$, where $\text{CR}_d \equiv R_{\text{hs}0}/R_{\text{hs},m}$ is the maximum hot-spot convergence ratio during shell deceleration and $R_{\text{hs}0}$ is the hot-spot radius at the beginning of deceleration. So, to decrease the instability drive term, CR_d should be decreased, but to reduce the ignition threshold, $R_{\text{hs},m}$ must also be reduced. This means that the deceleration phase should start later (i.e., at a smaller radius); therefore, $R_{\text{hs}0}$ needs to be reduced as well as CR_d .

Now we turn to scaling laws for CR_d and $R_{\text{hs}0}$ to identify the target design parameters that can achieve these desired reductions. It can be shown (following from Ref. 3) that

$$\text{CR}_d \sim \frac{v_{\text{imp}}^{2/3}}{\alpha_{\text{inf}}^{1/5} p_{\text{sh}0}^{2/15}}, \quad (1)$$

where v_{imp} is the peak implosion velocity, α_{inf} is the in-flight shell adiabat, and $p_{\text{sh}0}$ is shell pressure at the onset of deceleration. Also,

$$R_{\text{hs},m} = \frac{R_{\text{hs}0}}{\text{CR}_d} \sim R_0 \frac{p_0^{1/5} \alpha_{\text{inf}}^{1/5}}{p_{\text{sh}0}^{1/5} v_{\text{inf}}^{2/3}}, \quad (2)$$

where R_0 is the initial inner surface radius and p_0 is the initial vapor (central) pressure of the target. Equations (1) and (2) show that CR_d and R_{hs0} can be reduced by lowering the initial vapor pressure p_0 and/or increasing the shell pressure at the start of deceleration p_{sh0} . The remaining reduction in RT growth for the lower-central-density design comes from the increase in the ablative stabilization and reduction in the Atwood number.

Mass ablation from the inner shell surface, characterized by an ablation velocity v_a , reduces RT growth since the hot spot preferentially ablates the RT spikes that contact the hot spot at higher temperature gradients. It can be shown (following from Refs. 6 and 7) that

$$v_a \sim \frac{\alpha_{\text{inf}}^{0.5} v_{\text{imp}}^{2.2}}{R_0 p_0^{0.2} p_{\text{sh0}}^{0.13}}, \quad \frac{v_a}{R_{\text{hs,m}}} \sim \frac{\alpha_{\text{inf}}^{0.3} v_{\text{imp}}^{2.85}}{R_0^2 p_0^{0.4} p_{\text{sh0}}^{0.07}}. \quad (3)$$

As with the deceleration-phase convergence ratio and hot-spot radius at the onset of deceleration, the mass ablation velocity v_a increases with a lower initial vapor pressure. Meanwhile, density scale lengths L_m that are higher correspond to lower Atwood numbers A_T . Following from the previously written scaling laws and Ref. 6, it can be shown that

$$L_m \sim R_0 p_0^{0.2} p_{\text{sh0}}^{0.27} \alpha_{\text{inf}}^{0.8} v_{\text{imp}}^{0.54}, \quad \frac{L_m}{R_{\text{hs,m}}} \sim v_{\text{imp}}^{1.2} p_{\text{sh0}}^{0.33}. \quad (4)$$

Equation (4) shows that L_m is larger in designs with increased shell pressure at the onset of deceleration, p_{sh0} . Taken together, the scaling laws in Eqs. (1)–(4) for CR_d , R_{hs0} , v_a , and L_m show the beneficial stabilizing effects of reducing the initial vapor density and increasing the shell pressure at the start of the deceleration phase. This is accomplished most efficiently by reducing the initial vapor pressure p_0 . A lower initial vapor pressure leads to extra convergence of the central region necessary to build up its pressure and begin shell deceleration; then, because of the convergence effects, the shell pressure p_{sh0} at the beginning of deceleration increases as well. Furthermore, as will be shown in an upcoming paper, 1-D simulations in *LILAC*⁸ show that low-central-density designs experience reduced CR_d and R_{hs0} , as well as increased v_a and L_m . However, the fairly weak dependence of the hot-spot convergence ratio and stabilizing terms on the initial vapor density requires that it must be significantly reduced (factor of 5 or more). While this is not feasible with nominal cryogenic targets, the new dynamic shell formation concept can achieve this reduction by controlling the strength of the blast wave and the duration of the target expansion phase.⁹

To validate these predictions, we use 2-D hydrodynamic simulations in *DEC2D*¹⁰ to study perturbation amplification during shell deceleration for two dynamic shell designs driven by shorter and longer laser pulses. In Ref. 11, one can find details of the target dimensions and pulse shapes that produce central densities of 0.6 mg/cm³ and 0.12 mg/cm³, respectively. Figure 1 shows density maps for the two dynamic shell designs taken at times when the neutron production reaches $\dot{N} \cong 5 \times 10^{26} \text{ s}^{-1}$. The perturbation amplification is significantly reduced in the lower-central-density design [Fig. 1(b)] compared to the high-central-density design [Fig. 1(a)], despite the smaller hot-spot size, in agreement with the scaling arguments described earlier. Similarly, Fig. 2(a), which shows the mode $\ell = 20$ growth for the two dynamic shell designs, again confirms larger stabilization effects in the lower-density design. Figure 2(b) compares even-mode spectra for the two designs. The greatest RT growth suppression for the lower-density design occurs at mid- and higher-mode numbers, while the improvement for the low-mode numbers is slightly more modest.

Motivated by various scaling laws, we have demonstrated with 2-D simulations that reducing the initial central density in ICF targets leads to smaller hot spots (reducing hot-spot energies required for ignition) and, at the same time, suppresses deceleration RT growth. The required central-density reduction can be achieved using the new dynamic shell-formation concept. These results show a promising path to achieving ignition and high gains in laser-direct-drive designs at moderate laser energies $E_{\text{laser}} \sim 1 \text{ MJ}$.

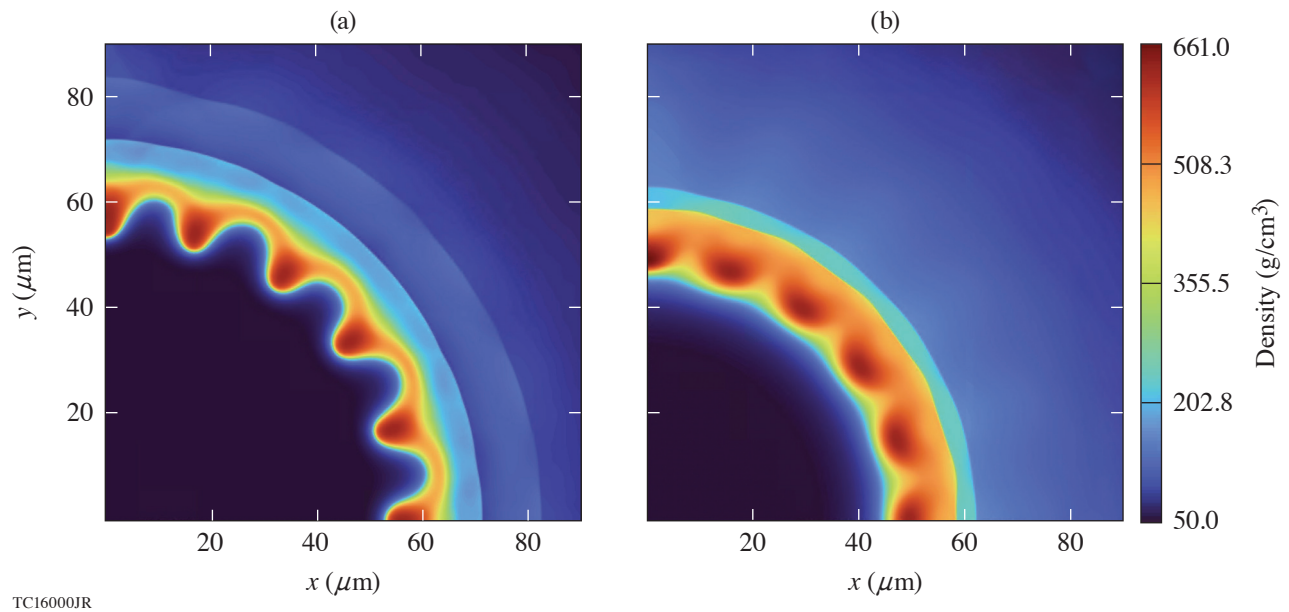


Figure 1

Two-dimensional density maps from mode $\ell = 20$ DEC2D simulations for the dynamic shell designs with (a) higher and (b) lower central densities (as described in Ref. 11), near stagnation at times of an equal neutron-production rate of $\dot{N} \cong 5 \times 10^{26} \text{ s}^{-1}$.

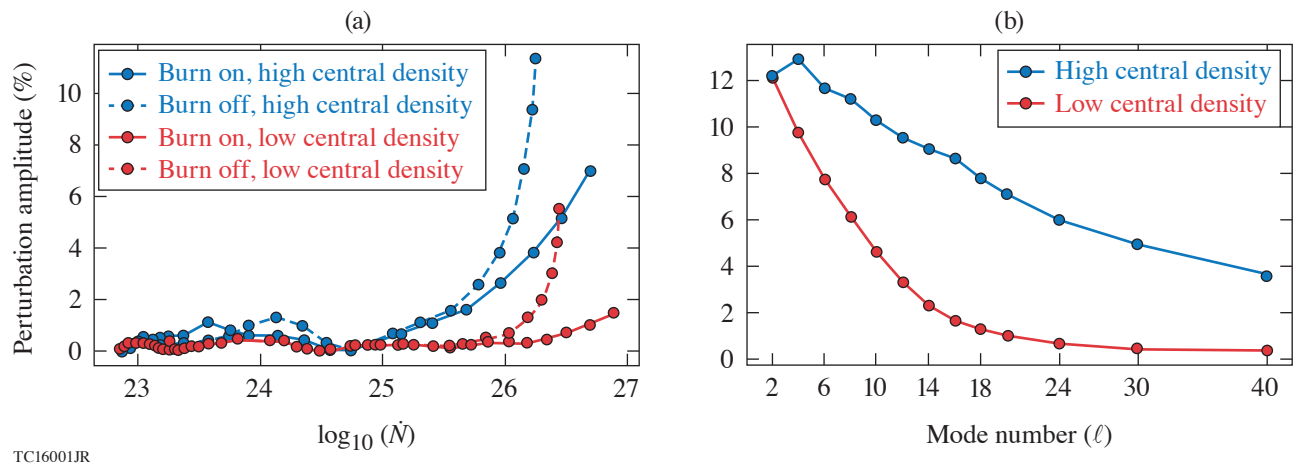


Figure 2

(a) Deceleration RT mode $\ell = 20$ evolution for dynamic shell designs with high/low central densities and alpha heating turned on or off. (b) Deceleration RT mode spectra with alpha heating turned on, taken at a neutron-production rate of $\dot{N} \cong 5 \times 10^{26} \text{ s}^{-1}$ for the dynamic shell designs with high/low central densities. (Lines are used to guide the eye and do not represent fits.)

Funding was provided by the ARPA-E BETHE Grants No. DEFOA-0002212 and DE-AR0001272 and DOE OFES Award No. DE-SC0017951. This material is based upon work supported by the Department of Energy National Nuclear Security Administration under Award Number DE-NA0003856, the University of Rochester, and the New York State Energy Research and Development Authority.

1. J. D. Lindl, *Inertial Confinement Fusion: The Quest for Ignition and Energy Gain Using Indirect Drive* (Springer, New York, NY, 1998).
2. S. Atzeni and J. Meyer-ter-Vehn, *The Physics of Inertial Fusion: Beam Plasma Interaction, Hydrodynamics, Hot Dense Matter*, 1st ed., International Series of Monographs on Physics, Vol. **125** (Oxford University Press, Oxford, 2004).
3. V. N. Goncharov *et al.*, Phys. Plasmas **21**, 056315 (2014).
4. V. N. Goncharov *et al.*, Plasma Phys. Control. Fusion **59**, 014008 (2017).
5. V. N. Goncharov *et al.*, Phys. Plasmas **7**, 5118 (2000).
6. R. Betti *et al.*, Phys. Plasmas **8**, 5257 (2001).
7. C. D. Zhou and R. Betti, Phys. Plasmas **14**, 072703 (2007).
8. J. Delettrez *et al.*, Phys. Rev. A **36**, 3926 (1987).
9. V. N. Goncharov *et al.*, Phys. Rev. Lett. **125**, 065001 (2020).
10. K. M. Woo *et al.*, Phys. Plasmas **25**, 052704 (2018).
11. W. Trickey *et al.*, Front. Phys. **9**, 784258 (2021).